Bull. nat. Hist. Mus. Lond. (Geol.) **57**(2): 95–107 Issued 29 November 2001

Gough's Cave 1 (Somerset, England): a study of the pectoral girdle and upper limbs

STEVEN E. CHURCHILL
Department of Biological Anthropology and Anatomy, Duke University, Durham NC 27708, USA

SYNOPSIS. The pectoral girdles, arms and forearms of Cheddar Man (Gough's Cave 1) are well preserved and, with the exception of a missing left scapula, are completely represented. These remains, which derive from early Holocene deposits in Gough's Cave, are described here. Comparative evaluation of the Gough's Cave 1 remains reveals that his upper limb skeleton was somewhat gracile, but certainly within the range of variation in strength measures of his contemporaries.

INTRODUCTION

The upper appendicular skeleton of Cheddar Man is represented by both claviculae, the right-side scapula, the humeri, ulnae and radii of both sides, and elements of both hands. The preservation of the upper limb elements is generally good.

The elements of the pectoral girdles, arms and forearms are described below (the manual remains are described elsewhere), followed by a discussion of the overall morphology of the upper limbs.

MATERIAL

The description of the Gough's Cave 1 upper limb remains includes both traditional osteometric (Tables 1, 2, 4–7, 9, 10, 12 and 13) and diaphyseal cross-sectional data (Tables 3, 8, and 11). Mean osteometric and cross-sectional data are provided for other European Mesolithic and later Upper Paleolithic specimens to provide a comparative framework for evaluating the morphology of Gough's Cave 1. These additional specimens range in geological age from the terminal Pleistocene to the mid-Holocene, and include Arene Candide 2 to 5, 10, and 12 to 15, Bruniquel 24, Cap-Blanc 1, Chancelade 1, Farincourt 1, Gramat 1, Hoëdic 1, 2, and 4 to 10, Neuessing 2, Oberkassel 1 and 2, Rochereil 1, Romito 3 and 4, Romanelli 1, St. Germain-la-Rivière 4, Téviec 1, 7 to 9, 11 and 16, and Veyrier 1 (Stasi & Regalia, 1904; Verworn *et al.*, 1919; Grazzini, 1921; Péquart & Péquart, 1934; Bonin, 1935; Boule & Vallois, 1937, 1946; Vallois, 1941–1946, 1972; Lacam *et al.*, 1944; Pittard & Sauter, 1945; Sauter, 1957; Graziosi, 1962; Genet-Varcin & Miquel, 1967; Billy, 1969; Gieseler, 1977; Paoli *et al.*, 1980). All comparative data were collected by the author on original specimens.

Diaphyseal cross-sections of the claviculae, humeri and ulnae were reconstructed from radiographs and external contour molds for the midshaft (claviculae and humeri) or mid-proximal (ulnae) diaphyses. Subperiosteal contour molds were taken perpendicular to the diaphyseal axis, using dental putty molds (Cuttersil Putty Plus: Heraeus Kulzer Inc.), at 50% (midshaft) or 65% (mid-proximal) of biomechanical length (measured from the distal end). The molds were photostatically reproduced on paper to provide the subperiosteal (outside) contour of the cross-section. In the case of claviculae, ventral, dorsal, superior and inferior cortical dimensions were measured from superoinferior and dorsoventral radiographs. For humeri and ulnae, anterior, posterior, medial and lateral cortical thicknesses were measured from mediolateral and anteroposterior radiographs. Subperiosteal dimensions from the original specimens were compared with those from the radiographs to determine the degree of parallax distortion and thus allow for algebraic correction of cortical thickness measurements. The cortical dimensions were used along with the subperiosteal contour to interpolate the endosteal contour. The resultant cross-sections were manually digitized and geometric properties were computed using a PC-DOS version (Eschman, 1990) of SLICE (Nagurka & Hayes, 1970).

SLICE calculates the total subperiosteal (TA) and cortical (CA) areas, 2nd moments of area about the superoinferior (clavicle) or anteroposterior (humerus and ulna) (I_x) and dorsoventral (clavicle) or mediolateral (humerus and ulna) (I_y) axes, and the maximum (I_{max}) and minimum (I_{min}) 2nd moments of area. Geometric analysis of cross-sections provides measures of the contribution of bone geometry to the resistance of biomechanical loads: in the case of cortical area, to axial compressive and tensile loads; for 2nd moments of area, to bending loads. Medullary area (MA) can be determined from total and cortical areas (MA = TA – CA). The polar moment of area (J, or I_p) is a measure of torsional rigidity and overall strength, and can be determined as the sum of any two perpendicular 2nd moments of area ($J = [I_x + I_y] = [I_{max} + I_{min}]$). Since cross-sectional measures of strength co-vary positively with body size, humeral and ulnar cross-sectional values were standardized by powers of bone length to produce measures of relative strength, or *robusticity*. Following the rationale described in Churchill (1994), measures of cross-sectional area (TA, CA and MA) were standardized as:

$$\text{AREA}_{\text{standardized}} = (\text{AREA}_{\text{unstandardized}}/\text{AL}^2) * 10^5$$

where AL = humeral or ulnar articular length. 2nd (and polar) moments of area (I_x, I_y, I_{max}, I_{min}, J) were similarly standardized as:

$$\text{2nd Moment}_{\text{standardized}} = (\text{2nd Moment}_{\text{unstandardized}}/\text{AL}^4) * 10^9.$$

In addition to the measures of bone rigidity outlined above, three cross-sectional shape indices were computed to better illustrate the morphology of the Gough's Cave 1 upper limb material. Percent cortical area (%CA = 100*CA/TA) serves as a simple measure of the degree of cortical occlusion of the medullary space. Ratios of 2nd moments of area provide information about diaphyseal shape (at the location of the cross section) with respect to anatomical axes (I_x/I_y) or with respect to the axis of maximum bending rigidity (I_{max}/I_{min}).

CLAVICULAR REMAINS

Both claviculae are preserved and are virtually complete (Figs 1, 2). Both lack the sternal epiphysis but have well preserved metaphyseal plates, making it clear that the sternal secondary centres of ossification were unfused. The right clavicle is damaged on the inferior and

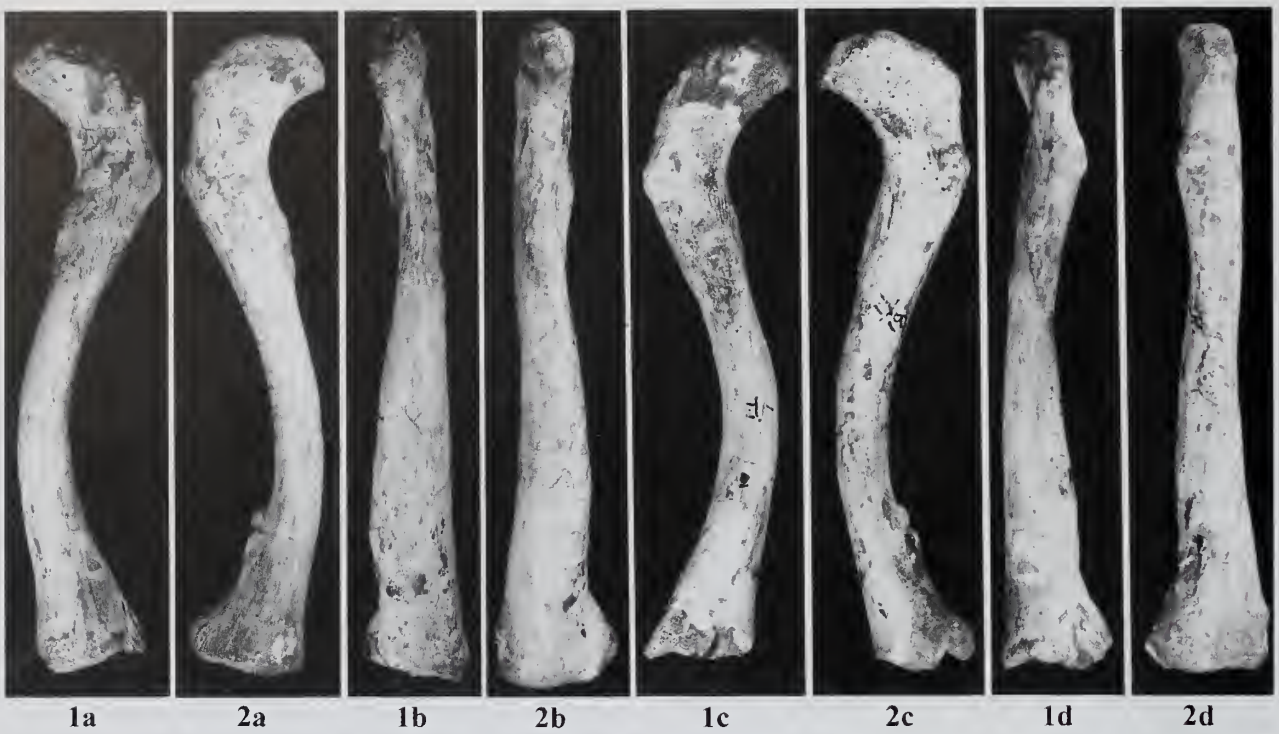

Figs 1, 2 Gough's Cave 1 claviculae, in superior (a), ventral (b), inferior (c) and dorsal (d) views; **1,** right-side clavicle; **2,** left-side clavicle; × 0.66.

dorsal aspects of the shaft around the costoclavicular ligament attachment area, and is patched with plaster in this location. The right-side bone also suffers from erosion and damage over the superior, dorsal and inferior surfaces of the acromial process. The left-side clavicle is undamaged.

Both claviculae are fairly short and stout and not markedly curved. The acromial ends are short and more curved than the proximal shafts, which have only a slight curvature. The sternal end of the right clavicle is round in medial view (with a maximum dorsoventral diameter of 20.9mm, and a maximum superoinferior diameter of 23.6mm), while the left is a dorsoventrally narrow oval (maximum DV diameter = 17.9mm, maximum SI diameter = 27.3mm). The right clavicle exhibits a greater degree of torsion in the shaft than the left clavicle. With the acromial processes held horizontally, in medial view the long axis of the articular surface (metaphyseal plate) of the right-side sternal end is inclined at a 45° angle (superoventral to inferodorsal) to the coronal plane. In the left clavicle, the long axis of the sternal articulation is also oriented superoventrally to inferodorsally, but it forms only a 15° angle with the coronal plane. The overall size and shaft curvatures is largely symmetrical between the sides (Table 1). The medial shafts are elongated superodorsal to inferoventral (*i.e.*, the long axes of the shaft cross-sections run in that direction).

The costoclavicular ligament attachment area (on the left clavicle, this area is obscured by plaster on the right clavicle) is a dorsoventrally narrow but mediolaterally long scar. The left-side costoclavicular ligament insertion area is dorsally placed, so much so that it is almost positioned on the dorsal surface of the shaft. On both sides the anterior medial shafts (in the vicinity of the *M. pectoralis major* attachment area) are flattened and are mostly smooth (there is some mild rugosity along the inferomedial edge of

Table 1 Dimensions (mm) of the Gough's Cave 1 claviculae.

	Right	Left
Maximum length (M-1)[a]	(135)	135.9
Articular length[a,b]	128.3	132.2
Conoid length[a,c]	102.9	104.4
Midshaft maximum diameter[d]	13.9	13.9
Midshaft minimum diameter[d]	9.6	9.8
Midshaft circumference (M-6)	40	39
Mid-proximal superoinferior diameter[e]	14.6	11.4
Mid-proximal anteroposterior diameter[e]	12.3	12.6
Mid-proximal circumference[e]	42	40
Proximal epiphyseal superoinferior diameter[f]	23.3	26.4
Proximal epiphyseal anteroposterior diameter[f]	22.7	18.2
Costal impression mediolateral diameter[g]	–	19.5
Costal impression dorsoventral diameter[g]	–	9.5
Conoid superoinferior diameter[h]	12.7	13.5
Conoid anteroposterior diameter[h]	17.7	17.8
Acromial superoinferior diameter[i]	11.5	11.7
Acromial anteroposterior diameter[i]	–	21.5

Martin numbers (M-#: Martin, 1928) for measurements are provided where appropriate.
[a] length lacking the unfused sternal epiphysis.
[b] direct distance between the mid-points of the proximal and distal epiphyses.
[c] direct distance from the mid-point of the proximal epiphysis to the middle of the conoid tubercle.
[d] midshaft determined relative to articular length.
[e] taken at mid-conoid length.
[f] maximum (SI-superoinferior) and minimum (AP-anteroposterior) diameters of the proximal epiphysis.
[g] mediolateral and dorsoventral diameters of the costoclavicular ligament attachment area.
[h] taken at the conoid tubercle perpendicular (SI) and parallel (AP) to the superior surface of the bone.
[i] acromial diameters taken perpendicular (SI) and parallel (AP) to the superior surface of the bone.

Table 2 Comparative clavicular osteometrics (mean, SD, n).

	Gough's Cave 1	LUP/Meso ♂	LUP/Meso ♀
Right claviculae			
Maximum length	(135)	143.4, 6.4, 8	129.4, 2.7, 5
Articular length	128.3	138.2, 6.7, 8	126.3, 3.6, 5
Conoid length	102.9	110.7, 2, 10	100.4, 7.6, 7
Mid-proximal SI diameter	14.6	11.8, 1.7, 10	9.8, 0.5, 7
Mid-proximal AP diameter	12.3	11.7, 0.8, 10	10.3, 0.9, 7
Conoid SI diameter	12.7	12.6, 3.7, 10	9.8, 1.4, 10
Conoid AP diameter	17.7	17.7, 1.9, 10	15.2, 1.8, 10
Left claviculae			
Maximum length	135.9	145.4, 9.0, 10	128.0, –, 2
Articular length	132.2	140.6, 9.1, 10	125.6, –, 2
Conoid length	104.4	109.6, 9.8, 13	98.8, 5.4, 4
Mid-proximal SI diameter	11.4	11.8, 2.1, 16	10.0, 0.8, 6
Mid-proximal AP diameter	12.6	11.7, 0.8, 16	9.8, 1.3, 6
Conoid SI diameter	13.5	11.0, 1.7, 15	10.0, 1.1, 8
Conoid AP diameter	17.8	17.2, 3.0, 15	14.2, 1.3, 7

All measurements are in mm and are defined in Table 1.

Table 3 Mid-shaft clavicular cross-sectional properties (mean, SD).

	Gough's Cave 1	LUP/Meso ♂ (n=4)	LUP/Meso ♀ (n=2)
Right claviculae			
Total area (TA) (mm^2)	124.9	107.4, 8.0	68.8
Cortical area (CA) (mm^2)	87.3	84.0, 7.8	57.0
Medullary area (MA) (mm^2)	37.6	23.4, 7.2	11.8
SI 2nd moment of area (I_x) (mm^4)	1319.8	869.5, 198.1	450.9
DV 2nd moment of area (I_y) (mm^4)	1154.2	884.1, 96.2	305.4
Maximum 2nd moment of area (I_{max}) (mm^4)	1752.1	1001.2, 131.3	473.0
Minimum 2nd moment of area (I_{min}) (mm^4)	721.9	752.5, 139.5	283.3
Polar moment of area (J) (mm^4)	2474.0	1753.7, 264.2	756.3
Percent cortical area (%CA)	69.9	78.3, 6.1	82.9
I_x/I_y	1.14	0.981, 0.185	1.487
I_{max}/I_{min}	2.43	1.343, 0.113	1.690
Left claviculae		(n=4)	(n=3)
Total area (TA) (mm^2)	118.9	122.0, 24.5	81.5, 17.9
Cortical area (CA) (mm^2)	73.9	91.2, 23.9	64.1, 13.1
Medullary area (MA) (mm^2)	45.0	30.8, 3.7	17.3, 5.1
SI 2nd moment of area (I_x) (mm^4)	999.6	1316.6, 671.8	559.3, 215.9
DV 2nd moment of area (I_y) (mm^4)	1084.4	1016.9, 325.7	498.9, 192.0
Maximum 2nd moment of area (I_{max}) (mm^4)	1505.1	1398.1, 626.5	591.6, 177.9
Minimum 2nd moment of area (I_{min}) (mm^4)	578.9	935.5, 364.1	466.7, 232.5
Polar moment of area (J) (mm^4)	2084.0	2333.5, 990.4	1058.3, 405.5
Percent cortical area (%CA)	62.2	74.2, 4.7	79.0, 2.2
I_x/I_y	0.92	1.240, 0.307	1.127, 0.081
I_{max}/I_{min}	2.60	1.468, 0.099	1.433, 0.517

See text for definition of measurements.

the *M. pectoralis major* origin area on the right-side bone; on the left-side there is some mild rugosity along the entire superior margin of the attachment area for this muscle). On the left clavicle there is a clearly defined insertion area for *M. sternocleidomastoideus*, beginning with a small but well defined projecting crest medially. This crest continues laterally as a narrow, mildly rugose strip extending about 25mm along the superior edge of the shaft. The right-side clavicle lacks a clearly marked insertion for *M. sternocleidomastoideus*, but instead has some poorly defined, mild rugosity in this area. On both sides, the *M. subclavius* attachment falls on a narrow ridge medially (between the *M. pectoralis major* origin area ventrally and the dorsal surface of the shaft dorsally) but broadens out as it nears the conoid tubercle on the proximal part of the acromial process. Here there is some mild rugosity (on the right, the left-side is largely non-rugose) and the attachment area is defined dorsally by a ridge running to and joining the conoid tubercle. There is also a slight ridge, more prominent in the right clavicle, separating the *M. subclavius* origin area ventrally from the *M. deltoideus* attachment area. The area of origin of *M. deltoideus* is weathered and damaged on the right-side, but on the left it can be seen as a well defined, rugose and projecting crest.

The conoid tubercles are large and project both inferiorly and dorsally. Both have long ridges extending medially from the tubercles (these ridges form the dorsal margins of the *M. subclavius* attachment areas). The trapezoid line on the left clavicle (this area is damaged on the right clavicle) is not overly rugose but is clearly visible. The acromial facets are poorly defined. The *M. trapezius* attachment areas are rugose on both acromial processes.

The Gough's Cave 1 claviculae are compared to those of late Upper Paleolithic and Mesolithic (LUP/Meso) males and females in Tables 2 and 3.

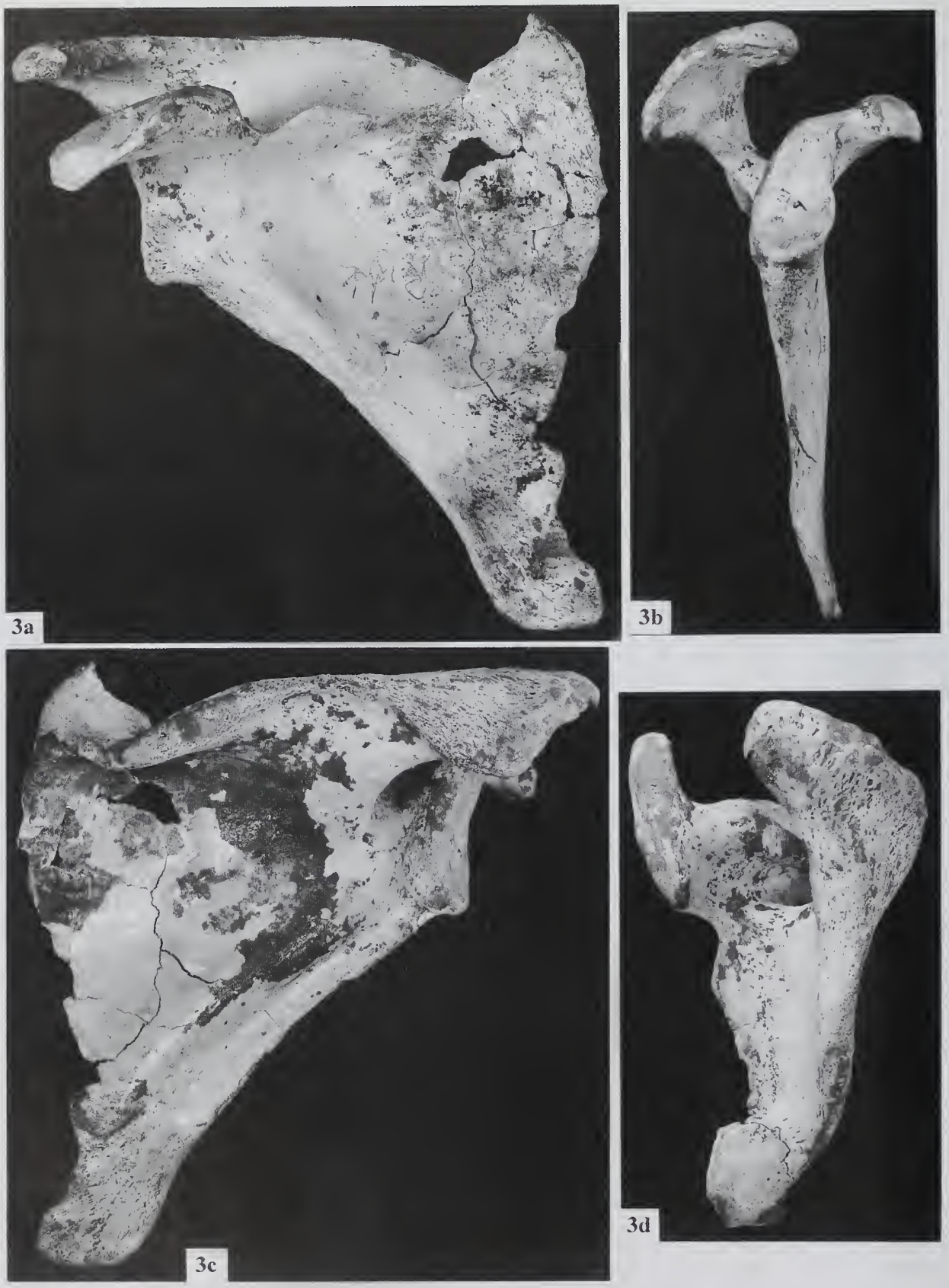

Fig. 3 Gough's Cave 1 right scapula, in ventral (a), lateral (b), dorsal (c) and superior (d) views; × 0.8.

SCAPULAR REMAINS

Only the right-side scapula is preserved (Fig. 3). The bone is largely complete, lacking only the superior angle (including some of the body on the *M. supraspinatus* surface) and vertebral border (and the adjacent 1-1.5cm of the body) from just distal of the root of the spine to the inferior angle. Scapular metrics are provided in Tables 4 and 5.

All of the observable secondary centres of ossification are fully fused and the epiphyseal lines are obliterated. These include the subcoracoid centre, the infraglenoid centre, the acromial centre, and the vertebral border centre (at least at the root of the spine – the only place this centre can be evaluated). It is possible that the vertebral border – inferior angle centre of ossification was not fully fused along its entire length, and that the preserved portion of the inferior angle represents an epiphyseal surface. Reconstructive materials obscure observation of the inferior angle, making evaluation of the state of fusion of the growth centre difficult.

The glenoid fossa is piriform (pear shaped) and has a very strong dorsal orientation. The dorsal margin of the articular surface rounds off onto the base along the dorsal edge, especially on the dorsoinferior margin. The articular surface of the glenoid fossa is irregular but there does not appear to be a central pit (McCown & Keith, 1939) (again, reconstructive materials obscure the articular morphology). The attachment for the glenoid labrum can be made out along the ventral margin of the articular surface, but disappears along the dorsal edge where the articular surface rounds off onto the base.

The infraglenoid tubercle begins as a very large attachment area on the dorsoinferior edge and dorsal part of the inferior edge of the glenoid. The tubercle is very large and elongated superoinferiorly (extending 32.6mm below the inferior margin of the glenoid fossa). The surface of the infraglenoid tubercle itself is finely rugose. The axillary crest (the attachment site for the fascia separating *M. subscapularis* and *M. teres minor*) is blunt and rounded, and runs along the dorsal portion of the axillary border for most of its length (Fig. 3b). At the distal end of the inferior *M. teres minor* attachment area the axillary crest veers dorsally and forms a rather strong crest on the dorsolateral edge of the axillary border. This morphology suggests that the *M. subscapularis* extended dorsally around the axillary border and had some fibres attached to the dorsal side of the lateral edge of the scapula at this level. The dorsal pillar (see Churchill, 1994) is laterally placed (running along the lateral-most edge of the axillary border) and well developed, and forms a deep sulcus on the body just medial of the pillar. The ventral pillar is medially positioned and is very strong, leaving a long, wide and shallow sulcus on the ventral aspect of the axillary border. Gough's Cave 1's scapular axillary border thus presents a ventral sulcus morphology similar to that seen in high frequencies in recent samples of European (and European-descent) populations (Trinkaus, 1977; Frayer, 1992; Churchill, 1996). On the dorsal aspect of the axillary border, there is what appears to be a vascular groove separating the infraglenoid tubercle and the superior portion of the attachment area for *M. teres minor*. This groove may indicate an accessory artery in the scapular anastomotic complex, one arising either from the root of the subscapular artery or perhaps stemming directly from the axillary artery. The groove for the circumflex scapular artery can be seen clearly dividing the *M. teres minor* origin further distally on the border. The *M. teres minor* attachment areas are poorly defined, the superior attachment area is not flattened and neither area is rugose. There is a small lateral flange for *M. teres major* and some flattening of the distal end of the axillary border.

There is little-to-no curvature of the body of the scapula. With the scapula held in anatomical position, the lateral edge of the acromion is broad dorsoventrally (measuring 49mm). The lateral edge of the acromion bears a rugose strip for the attachment of *M. deltoideus* along its entire length. The superior/dorsal surface of the spine is sinuous. The *M. trapezius* insertion area is not rugose. On the coracoid process, the lateral edge bears two small depressions with small crests for the *M. coracobrachialis* and *M. biceps brachii* short head attachments. The scapular notch is relatively broad.

Table 4 Dimensions (mm) of the Gough's Cave 1 right scapula.

Morphological length (M-2)	100.0
Infraspinatus breadth (M-5a)	124.0
Basal spinous length (M-8)	79.4
Spino-acromial length[a]	130.0
Spinal thickness[b]	11.5
Acromio-glenoid distance[c]	45.4
Axillary border length (M-3)	126.6
Functional axillary border length[d]	139.0
Mid-axillary border thickness[e]	12.5
Spino-glenoid angle (M-22)	86°
Axillo-glenoid angle (M-17)	35°
Axillo-spinal angle (M-16)	60°
Glenoid maximum length (M-12)	38.0
Glenoid maximum breadth (M-13)	26.1
Glenoid articular length[f]	34.7
Glenoid articular breadth[f]	24.8

Martin numbers (M=#: Martin, 1928) for measurements are provided where appropriate.
[a] vertebral border at the spine to the tip of the acromion.
[b] maximum superoinferior thickness along the middle of the spine.
[c] center of glenoid fossa to the tip of the acromion.
[d] center of glenoid fossa to the most caudal point on the inferior angle.
[e] dorsoventral diameter of the mid-axillary border, including dorsal and ventral pillars as present.
[f] glenoid fossa length and breadth taken across the internal margins of the glenoid labrum attachment.

HUMERAL REMAINS

Both humeri are virtually complete (Figs 4, 5). The right-side has some damage to the dorsal surface of the head and this area is filled in with plaster. The left-side has some erosion to the medial surface of the head and what appears to be an erosional defect on the superoventral surface of the trochlea (see below). Otherwise, the two bones are very well preserved.

There is a very slight trace of an epiphyseal line on the anterior and medial surfaces of the proximal metaphysis just below the lesser tubercle and the articular surface of the head. The line is more apparent on the right humerus than on the left. On both humeri the line is largely obliterated on the dorsal and lateral surfaces. Even though the line is visible, the head is fully fused and the lines are near obliteration. Distally, the distal epiphyses and the medial epicondyle secondary centres of ossification are fully fused and the lines obliterated on both humeri.

The two sides are largely symmetrical with respect to size, robusticity and most details of morphology (Table 6). Although both humeri are similar in size and rugosity of muscle markings, the left-side seems to be the generally more muscle marked of the two. The humeri are not markedly robust. There is no notable curvature to the diaphyses in any plane. The deltoid tuberosities are neither large nor projecting, such that the diaphyses are of uniform dimension (save for a slight swelling at the deltoid tuberosity) along the shaft from every perspective. The head of the right humerus is dorsomedially directed (producing a torsion angle of 141°), while the left has a more medially oriented head (torsion angle = 166°).

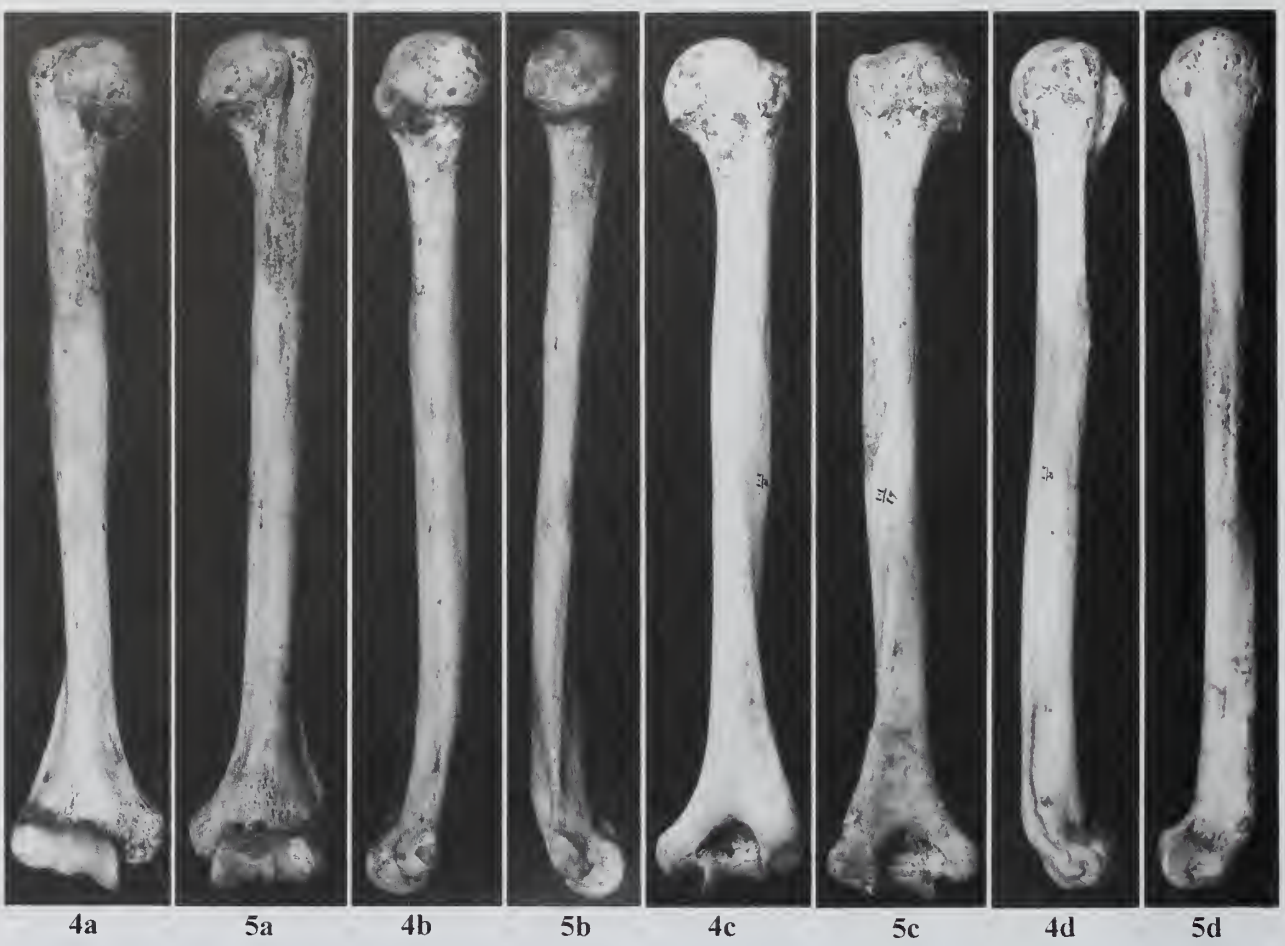

Figs 4, 5 Gough's cave 1 humeri in ventral (a), medial (b), dorsal (c) and lateral (d) views; **4,** right-side humerus; **5,** left-side humerus; × 0.37.

Table 5 Comparative scapular dimensions (mean, SD, n)

	Gough's Cave 1 (right)	LUP/Meso ♂ (right + left)	LUP/Meso ♀ (right + left)
Morphological length	100.0	139.4, 34.6, 4	–
Axillary border length	126.6	129.9, 5.6, 9	123.0, – , 2
Glenoid articular length	34.7	35.7 2.5, 8	32.1, 1.7, 7
Glenoid articular breadth	24.8	26.6, 1.7, 6	23.1, 1.4, 7
Glenoid index[a]	71.5	73.7, 2.2, 6	72.1, 4.1, 7

All measurements are in millimeters and are defined in Table 4.
[a] Glenoid index = (articular breadth/articular length) x100.

The articular surfaces of the heads are fairly round, the left-side seems to be somewhat more oval shaped (with the long axis running superoinferiorly) than the right. The articular surfaces are smooth (save for erosional damage) and free of any signs of degeneration.

The right humerus has some erosion over the lateral surface of the greater tubercle, and the only muscle attachment area not eroded is the 'facet' for the insertion of *M. teres minor*. On the left-side the greater tubercle is well preserved, revealing a distinct 'facet' for *M. teres minor* and a more diffuse attachment area for *M. supraspinatus* and *M. infraspinatus*. The attachment area for these muscles is smooth and there is no clear separation between the facets for the two muscles. Both sides have pronounced intertubercular sulci formed medially by superoinferior running pillars extending from the lesser tuberosities along the insertion areas for *M. latissimus dorsi* and *M. teres major*, and laterally by pronounced crests for *M. pectoralis major*. The pillars are non-rugose (except at the muscle attachment areas) and the *M. pectoralis major* scars are only mildly rugose.

The deltoid tuberosities are not pronounced, but appear instead as slightly projecting, rugose crests. Indentations can be seen on both sides at the intersection of the proximal deltoid tuberosity with the inferior portion of the attachment of the pectoralis major muscle (the indentation is sightly more pronounced on the right-side). The indentation is best seen in medial or lateral view (Figs 4b, 4d, 5b, 5d). On the right-side there is a very slight musculoskeletal stress marker

Table 6 Dimensions (mm) of the Gough's Cave 1 humeri.

	Right	Left
Maximum length (M-1)	322	322
Articular length (M-2)	316	318
Midshaft maximum diameter (M-5)	22.2	21.9
Midshaft minimum diameter (M-6)	17.0	15.2
Midshaft circumference (M-7a)	65	63
Distal minimum circumference (M-7)	62	61
Head anteroposterior diameter (M-10)	(40.2)	40.1
Epicondylar breadth (M-4)	58.0	57.5
Distal articular breadth (M-12a)	43.0	43.0
Capitular breadth (M-12)	21.0	19.0
Trochlear breadth (M-11)	20.2	21.1
Trochlear max. anteroposterior diam.(M-13)	24.9	23.9
Medial epicondyle projection[a]	18.3	16.7
Lateral epicondyle projection[b]	19.7	20.1
Olecranon fossa breadth (M-14)	23.8	23.9
Olecranon fossa depth (M-15)	12.2	12.2
M. pectoralis major sulcus breadth[c]	5.9	5.6
Deltoid tuberosity width[d]	11.5	13.3
Deltoid tuberosity circumference[e]	68	64
Cubital angle (M-16)	113°	101°
Torsion angle (M-18)	141°	166°

Martin numbers (M-#: Martin, 1928) for measurements are provided where appropriate.
[a] medial trochlear margin to the most projecting portion of the epicondyle.
[b] lateral trochlear margin to the most projecting tip of the epicondyle.
[c] maximum breadth (mediolateral) of the middle of the muscle insertion area.
[d] distance between the apices of the delimiting crests of the tuberosity taken at 5/12's of humeral maximum length, following Endo (1971).
[e] shaft circumference taken at 5/12's of humeral maximum length, following Endo (1971).

('enthesopathy': Dutour, 1986; Hawkey & Merbs, 1995) in the anterior crest of the deltoid just inferior of this depression. A similar but smaller projection can be seen at the same location on the left-side. The deltoid tuberosities are narrow in anterolateral view and are two-crested on both humeri. The posterior crest on the left humerus is more rugose than the posterior crest on the right humerus (the right-side crest is very mildly rugose).

The other muscle attachment areas on the shaft are non-rugose (including *M. brachialis*, and the medial and lateral heads of *M. triceps brachii*). There is some slight rugosity along the *M. coraco-brachialis* insertions on both humeri.

Distally, the medial epicondyles are very large in superoinferior dimension but do not project very far mediolaterally, giving them a squat appearance. Both medial epicondyles present smooth but irregular surfaces where the common flexor tendon attaches. On the left-side there is a distinct crest on the anterosuperior edge of the attachment area, between the medial epicondyle proper and the shaft of the humerus. No such crest is apparent on the right-side. The lateral supracondylar ridges also seem well developed. The common extensor tendon origins are represented by small, smooth areas, and the *M. anconeus* origins are represented on both sides by smooth, thin semi-circular ridges that do not join the common extensor attachment areas.

The distal articular surfaces are relatively small, and have deep medial and lateral grooves. The lateral grooves (separating the lateral trochlear margin from the capitulum) are very wide and distinct. The capitullae are very small superoinferiorly and are slightly indented on their inferolateral surfaces, giving them a slightly laterally pointed appearance in anterior view. The left trochlea has an oval eroded patch (measuring 13mm mediolaterally by 9.5mm superoinferiorly) on its anterosuperior surface. This appears to be post-mortem in nature, and there is no corresponding defect on the left ulna, ruling out osteoarthritic eburnation. No other signs of degeneration are present on the distal articulations.

From the dorsal perspective, the distal medial pillars are relatively broad. The lateral pillars are also broad, and the surfaces behind the capitullae are flat and at angles of ca. 145° to the dorsal surfaces of the lateral pillars. The olecranon fossae are relatively small but deep.

Comparative data on other late Pleistocene/early Holocene human humeri are provided in Tables 7 and 8.

Table 7 Comparative humeral osteometrics (mean, SD, n).

	Gough's Cave 1	LUP/Meso ♂	LUP/Meso ♀
Right humeri			
Maximum length[a]	322	307.3, 12.9, 17	287.0, 13.7, 9
Midshaft maximum diameter	22.2	23.9, 1.8, 17	20.7, 1.8, 10
Midshaft minimum diameter	17.0	17.7, 1.0, 17	15.4 1.6, 10
Distal minimum circumference	62	64.1, 4.1, 18	55.3, 5.2, 9
Head anteroposterior diameter	(40.2)	43.6, 2.8, 13	37.8, 3.2, 7
Epicondylar breadth	58.0	61.9, 2.2, 16	56.4, 2.9, 4
Distal articular breadth	43.0	42.8, 2.4, 16	39.2 4.3, 7
Deltoid tuberosity width	11.5	17.2, 2.8, 17	13.8, 2.2, 11
Deltoid tuberosity circumference	68	71.5, 3.9, 16	62.5, 4.4, 11
Left humeri			
Maximum length[a]	322	313.4, 12.1, 12	287.4, 7.5, 10
Midshaft maximum diameter	21.9	23.4, 2.5, 13	20.2, 1.2, 9
Midshaft minimum diameter	15.2	17.0, 2.0, 14	15.8, 1.0, 9
Distal minimum circumference	61	62.7, 5.7, 12	55.9, 2.6, 8
Head anteroposterior diameter	40.1	43.1, 1.6, 14	39.2, 1.5, 5
Epicondylar breadth	57.5	61.1, 3.1, 11	54.7, 1.8, 7
Distal articular breadth	43.0	43.2, 2.1, 10	38.5, 2.5, 7
Deltoid tuberosity width	13.3	16.9, 3.4, 13	13.6, 2.3, 10
Deltoid tuberosity circumference	64	69.5, 6.7, 13	59.7, 3.8, 10

All measurements are in millimeters and are defined in Table 6.
[a] includes estimated lengths for some comparative specimens

Table 8 Mid-shaft humeral cross-sectional properties, standardized[a] (mean, SD).

	Gough's Cave 1	LUP/Meso ♂ (n=17)	LUP/Meso ♀ (n=10)
Right humeri			
Total area (TA)	307.3	363.2, 59.4	314.7, 36.0
Cortical area (CA)	221.1	260.8, 52.1	224.4, 43.2
Medullary area (MA)	86.2	102.4, 32.5	90.2, 26.2
ML 2nd moment of area (I_x)	682.6	955.0, 296.5	789.7, 192.7
AP 2nd moment of area (I_y)	783.9	1104.0, 404.6	750.1, 207.5
Maximum 2nd moment of area (I_{max})	952.4	1241.1, 487.1	1048.9, 292.4
Minimum 2nd moment of area (I_{min})	514.1	718.5, 232.8	531.2, 153.7
Polar moment of area (J)	1466.5	2059.1, 684.7	1539.8, 384.5
Percent cortical area (%CA)	71.9	71.7, 8.0	70.2, 8.3
I_x/I_y	0.871	0.893, 0.132	1.079, 0.168
I_{max}/I_{min}	1.853	1.712, 0.313	1.901, 0.426
Left humeri		(n=12)	(n=9)
Total area (TA)	271.1	350.3, 59.9	297.7, 32.0
Cortical area (CA)	180.2	253.4, 53.6	207.0, 32.6
Medullary area (MA)	90.9	96.8, 29.3	90.7, 33.9
ML 2nd moment of area (I_x)	452.3	832.2, 251.9	659.2, 145.2
DV 2nd moment of area (I_y)	649.0	1106.7, 423.3	662.0, 152.4
Maximum 2nd moment of area (I_{max})	723.9	1313.3, 412.9	811.6, 187.8
Minimum 2nd moment of area (I_{min})	377.4	730.0, 246.7	473.5, 91.8
Polar moment of area (J)	1101.3	1938.8, 659.3	1321.2, 275.9
Percent cortical area (%CA)	66.5	72.2, 7.3	71.2, 10.7
I_x/I_y	0.697	0.803, 0.201	1.006, 0.184
I_{max}/I_{min}	1.918	1.837, 0.318	1.695, 0.136

See text for definition of measurements.

[a] Cross-sectional strength measures standardized to humeral articular length (HAL). Areal measures (TA, CA and MA) were divided by HAL^2 and multiplied by 10^5. 2nd moments of area (I_x, I_y, I_{min}, I_{max}, J) were divided by HAL^4 and multiplied by 10^9.

Table 9 Dimensions (mm) of the Gough's Cave 1 ulnae.

Measurement	Right	Left
Maximum length (M-1)	–	(270)
Articular length (M-2)	–	250
Olecranon length (M-8)	14.8	–
Olecranon height (M-7)	27.7	–
Olecranon breadth (M-6)	24.0	–
Trochlear notch chord (M-7(1))	23.5	–
Coronoid height[a]	36.3	34.9
Radial facet maximum diameter[b]	19.9	18.3
Radial facet minimum diameter[b]	10.9	10.6
Coronal trochlear angle (M-15)	14°	–
Diaphyseal sagittal trochlear angle (M-15a)	21°	–
Proximal anteroposterior diameter[c]	18.3	18.4
Proximal transverse diameter[c]	18.8	18.7
Proximal circumference[c]	51	49
Crest anteroposterior diameter (M-11)	15.3	13.7
Crest mediolateral diameter (M-12)	14.3	15.0
Midshaft anteroposterior diameter	12.2	12.2
Midshaft mediolateral diameter	–	13.2
Midshaft circumference	–	42
Distal minimum circumference (M-3)	37	–
Pronator quadratus crest maximum diameter[d]	12.8	–
Pronator quadratus crest minimum diameter[d]	10.6	–
Pronator quadratus circumference[d]	38	–
Head breadth[e]	16.9	17.0

Martin numbers (M-#: Martin, 1928) for measurements are provided where appropriate.

[a] maximum anteroposterior diameter from the dorsal surface of the bone to the anterior tip of the coronoid process (McHenry *et al.*, 1976).

[b] maximum and minimum diameters of the articular facet for the radial head.

[c] taken at the level of the distal border of the ulnar tuberosity (McHenry *et al.*, 1976).

[d] shaft maximum and minimum diameters and circumference at the most projecting portion of the pronator quadratus crest.

[e] mediolateral diameter of the ulnar head.

ULNAR REMAINS

Both ulnae are largely complete (Figs 6, 7, Table 9). The right-side is somewhat better preserved than the left, but is missing a 4cm portion of the diaphysis from about midshaft distally. This area has been reconstructed in plaster. With the exception of the missing diaphyseal fragment, the bone is complete. The left-side is missing the anterior half of the olecranon process (from the anterior edge of the *M. triceps brachii* insertion), including some of the olecranon articular surface in the trochlear notch. There is also some damage to the surface of the left-side distal shaft in the region of the *M. pronator quadratus* crest. Otherwise, the bone is very well preserved.

The proximal and distal epiphyses are fully fused. The left-side ulna has a closed but still (barely) visible epiphyseal line between the head and shaft. All of the other epiphyseal lines are fully obliterated.

Both ulnae are of moderate robusticity (Tables 10 and 11). The right-side shaft has a lateral curve to the distal end (as seen in volar view), beginning in the area around the *M. pronator quadratus* crest. The left-side diaphysis is straight, but has had some damage to and refitting of the distal end, perhaps affecting the appearance of distal shaft. The shafts are also straight in lateral view.

The trochlear notch on the right-side (the left is damaged) opens anteroproximally (Fig. 8). Neither side has a very marked separation (as either a crest or sulcus) between the coronoid and olecranon articular surfaces in the notch, nor does either side express a sagittally oriented crest in the notch. There is no evidence of degenerative changes to the trochlear or radial notches of either side. The radial notches are relatively large, and are oriented superolaterally.

The *M. triceps brachii* insertion on the olecranon process is mildly rugose (on the right ulna, this region can't be fully evaluated in the left), with vertical striations on the posterior edge of the olecranon but no spurring or indications of musculoskeletal stress lesions. The

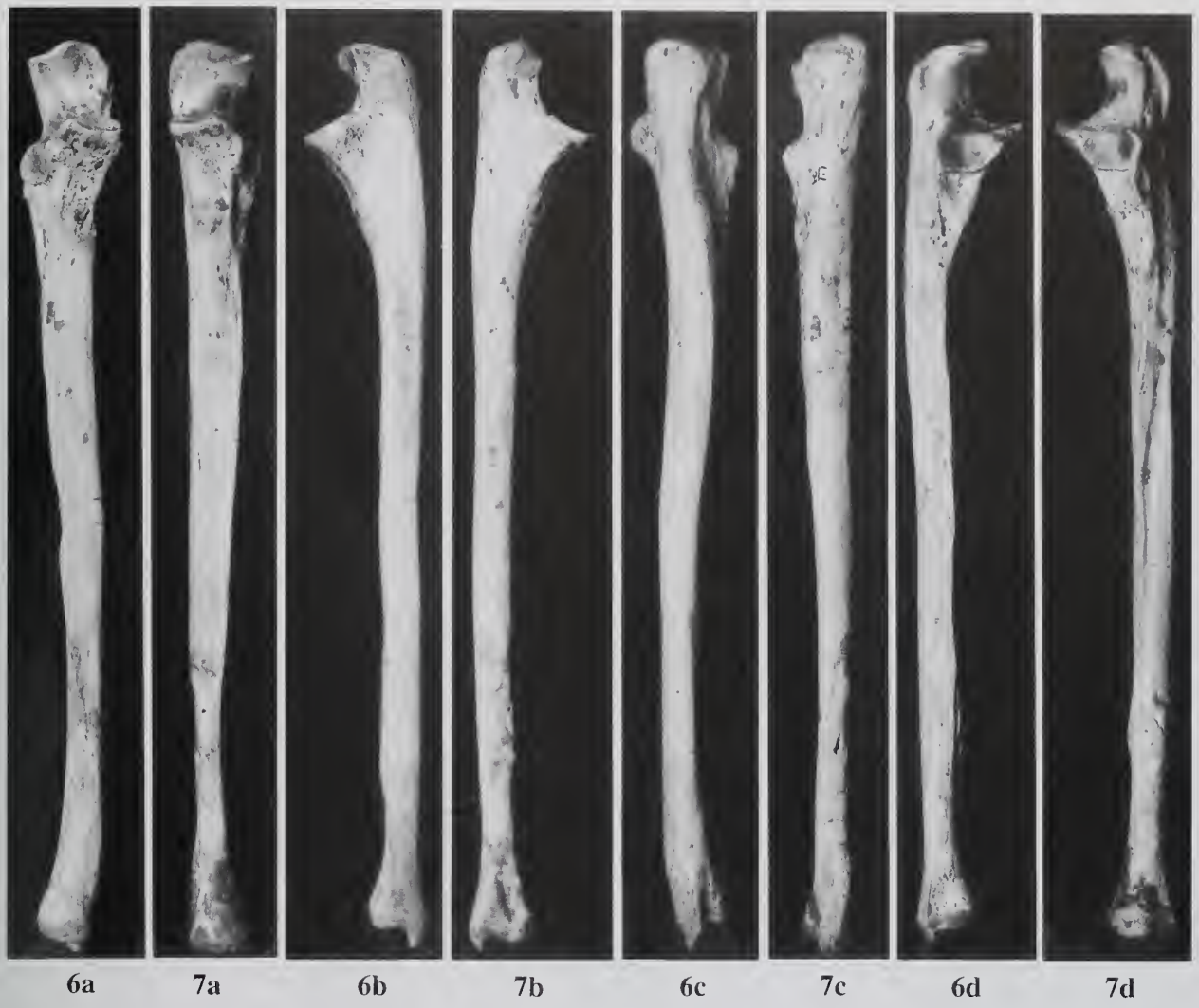

Figs 6, 7 Gough's Cave 1 ulnae, in ventral (a), medial (b), dorsal (c) and lateral (d) views; **6,** right-side ulna; **7,** left-side ulna; × 0.5.

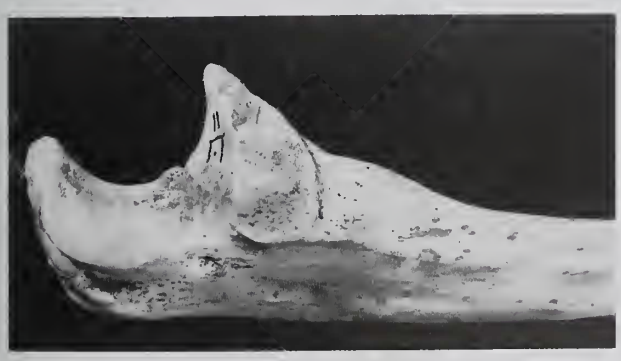

Fig. 8 Gough's Cave 1 right ulna in lateral view; × 1.

M. anconeus insertion area is mildly rugose, occupying a narrow ridge (between the medial and lateral surfaces of the proximal shaft) on the dorsal surface of the shaft. This mildly rugose line continues distally until it joins with the line marking the aponeurotic attachment of *M. flexor digitorum profundus*, *M. flexor carpi ulnaris* and *M. extensor carpi ulnaris*. Supinator crests of both sides are well developed, beginning as pronounced crests arising from the inferodistal margins of the radial notches (Fig. 8). The crests continue distally to a half centimeter or so below the *M. brachialis* scar, where they stop and then resume again another 10–20mm distally. The distal portions of the *M. supinator* ridges follow the interosseous crests (lying just posterior to and on the lateral surface of the interosseous crests), about one-third of the way down the shaft. The posterior edge of the proximal portion of the *M. supinator* attachment area is also marked by a crest on the lateral surface below the trochlea. The *M. brachialis* scars are moderately rugose, and present themselves as small raised patches (roughly 13mm proximodistally × 9mm mediolaterally on both sides). The area between the scars and the coronoid processes is mildly rugose. No markings are evident on either side for *M. pronator teres*. There is a large tubercle present on the anteromedial corner of the coronoid process in the area of the origin of the ulnar head of *M. flexor digitorum superficialis* on the right-side. This area is somewhat damaged in the left-side ulna, but it is certain that the tubercle, if indeed it existed, was not nearly as large as that of the right.

Table 10 Comparative ulnar osteometrics (mean, SD, n).

	Gough's Cave 1	LUP/Meso ♂	LUP/Meso ♀
Right ulnae			
Olecranon length	14.8	17.1, 2.6, 15	16.7, 2.0, 4
Olecranon height	27.7	27.1, 1.9, 13	23.8, 1.4, 4
Olecranon breadth	24.0	25.7, 1.3, 12	23.6, 1.1, 4
Trochlear notch chord	23.5	27.0, 3.6, 10	22.7, 2.7, 3
Coronoid height	36.3	37.4, 1.6, 12	32.2, 2.1, 6
Radial facet maximum diam	19.9	16.8, 1.8, 9	16.4, –, 2
Radial facet minimum diam	10.9	11.6, 0.6, 9	11.2, –, 2
Proximal AP diameter	18.3	15.7, 1.6, 13	15.2, 2.0, 5
Proximal transverse diam	18.8	16.8, 2.0, 13	13.7, 1.7, 5
Proximal circumference	51	50.5, 3.8, 12	45.0, 2.6, 5
Midshaft AP diameter	12.2	14.6, 1.9, 5	12.8, –, 1
Pron. quadratus max diam	12.8	13.6, 1.4, 11	12.1, 1.2, 4
Pron. quadratus min diam	10.6	10.3, 0.9, 11	9.6, 0.9, 4
Pron. quadratus circum	38	38.9, 3.1, 11	35.3, 2.9, 4
Left ulnae		UP/Meso ♂	UP/Meso ♀
Maximum length[a]	(270)	263.9, 10.6, 14	245.8, 8.3, 4
Articular length[a]	250	241.6, 10.6, 15	224.7, 7.4, 7
Coronoid height	34.9	36.7, 1.1, 12	33.3, 1.0, 4
Radial facet maximum diam	18.3	16.8, 1.3, 9	16.4, 1.6, 3
Radial facet minimum diam	10.6	11.1, 1.2, 9	10.1, 0.4, 4
Proximal AP diameter	18.4	15.5, 2.2, 11	15.4, 1.6, 8
Proximal transverse diam	18.7	15.3, 2.8, 11	13.4, 1.7, 8
Proximal circumference	49	48.0, 6.3, 11	44.2, 3.5, 7
Midshaft AP diameter	12.2	15.2, 1.2,3	13.5, 0.6, 4
Midshaft ML diameter	13.2	14.5, 1.5, 3	11.7, 0.5, 4

All measurements are in millimeters and are defined in Table 9.
[a] includes estimated lengths for some comparative specimens.

Table 11 Mid-proximal ulnar cross-sectional properties, standardized[a] (mean, SD).

	Gough's Cave 1	LUP/Meso ♂ (n=4)	LUP/Meso ♀ (n=2)
Right ulnae			
Total area (TA)	228.8	266.8, 36.7	192.0
Cortical area (CA)	210.1	222.7, 33.3	177.1
Medullary area (MA)	18.7	44.1, 14.7	14.9
ML 2nd moment of area (I_x)	417.9	534.8, 235.8	352.3
AP 2nd moment of area (I_y)	491.5	655.3, 143.7	278.3
Maximum 2nd moment of area (I_{max})	536.8	714.5, 184.3	360.9
Minimum 2nd moment of area (I_{min})	372.7	475.6, 150.0	269.8
Polar moment of area (J)	909.5	1190.1, 325.7	630.7
Percent cortical area (%CA)	91.8	83.5, 5.5	92.5
I_x/I_y	0.850	0.814, 0.306	1.269
I_{max}/I_{min}	1.440	1.528, 0.203	1.338
Left ulnae		(n=3)	(n=3)
Total area (TA)	221.8	277.7, 17.2	244.0, 19.3
Cortical area (CA)	195.7	242.9, 27.4	221.6, 23.5
Medullary area (MA)	26.1	34.8, 24.5	22.5, 12.6
ML 2nd moment of area (I_x)	335.7	632.9, 187.8	562.9, 86.1
DV 2nd moment of area (I_y)	487.3	676.1, 141.1	443.4, 120.3
Maximum 2nd moment of area (I_{max})	488.9	784.4, 129.1	610.4, 110.3
Minimum 2nd moment of area (I_{min})	334.2	524.6, 79.4	395.9, 52.6
Polar moment of area (J)	823.1	1309.1, 179.3	1006.3, 160.4
Percent cortical area (%CA)	88.2	87.5, 8.7	90.8, 5.0
I_x/I_y	0.689	0.975, 0.376	1.319, 0.331
I_{max}/I_{min}	1.463	1.507, 0.267	1.537, 0.124

See text for definition of measurements.
[a] Cross-sectional strength measures standardized to ulnar articular length (UAL). Areal measures (TA, CA and MA) were divided by UAL^2 and multiplied by 10^5. 2nd moments of area (I_x, I_y, I_{min}, I_{max}, J) were divided by UAL^4 and multiplied by 10^9.

On both sides, the distal end of the interosseous crest branches into two crests – more strongly so on the right-side but also to some extent on the left. This may reflect a division of the membranes for *M. flexor digitorum profundus* anteriorly and *M. extensor indicus* posteriorly. The right-side *M. pronator quadratus* crest (this area is damaged in the left ulna) is relatively small but is clearly discernable as a narrow, projecting crest.

The styloid processes are relatively long. There are no signs of any degenerative changes to the distal articular surfaces on either side.

Table 12 Dimensions (mm) of the Gough's Cave 1 radii.

Measurement	Right	Left
Maximum length (M-1)	–	248
Articular length (M-2)	–	235
Proximal anteroposterior diameter[a]	13.5	13.1
Proximal mediolateral diameter[a]	12.2	12.8
Proximal circumference[a]	41	41
Crest anteroposterior diameter (M-5)	12.4	11.7
Crest mediolateral diameter (M-4)	17.1	15.6
Midshaft anteroposterior diameter (M-5a)[b]	12.0	11.9
Midshaft mediolateral diameter (M-4a)[b]	16.9	15.1
Midshaft circumference (M-5(5))[b]	46	42
Distal minimum circumference (M-3)	41	(41)
Head-neck length (M-1a)	33.0	31.3
Neck-shaft angle (M-7)	6°	6°
Head anteroposterior diameter (M-5(1))	21.1	22.4
Head mediolateral diameter (M-4(1))	21.2	21.3
Head circumference (M-5(3))	69	71
Neck anteroposterior diameter (M-5(2))	14.7	15.1
Neck mediolateral diameter (M-4(2))	12.4	14.7
Neck circumference (M-5(4))	44	46
Bicipital tuberosity length[c]	22.4	21.5
Bicipital tuberosity breadth[d]	14.1	14.2
Distal breadth (M-5(6))	–	27.7
Distal depth[e]	–	15.4
Carpal articular breadth[f]	–	27.3

Martin numbers (M-#: Martin, 1928) for measurements are provided where appropriate.
[a] taken midway between the bicipital tuberosity and the proximal end of the interosseous crest.
[b] right-side midshaft position was estimated using the more complete left-side radius.
[c] maximum proximodistal diameter of the tuberosity.
[d] maximum dorsovolar diameter of the tuberosity.
[e] maximum dorsovolar diameter of the distal epiphysis, not including the dorsal (Lister's) tubercle.
[f] maximum mediolateral diameter of the articular surface.

RADIAL REMAINS

Both radii are preserved (Figs 9, 10). The right radius is missing the distal end from the region of the distal interosseous crest. The diaphysis has also been broken and refitted near midshaft. The left-side is more complete but has some damage to its distal end. The anterior surface of the left distal shaft, from slightly below midshaft to the epiphyseal end, is eroded and damaged, and the anterior surface of the distal metaphyseal area is missing. The proximal halves of both radii are in a good state of preservation.

The proximal (right and left) and distal (left) epiphyses are fully fused and the epiphyseal lines are obliterated. No degenerative changes are evident in any of the preserved articular surfaces.

The heads of both radii are slightly (but only slightly) oblong, with the long axis running anteromedial to posterolateral. The neck of the right radius is narrower in both anterior and lateral views compared to the left (Table 12). The radial tuberosity and anterior oblique crest also have a slightly greater development on the left-side. The radial tuberosities are proximodistally short (Table 12), miderately wide, but projecting medially (the left more so than the right). The anterior oblique crests extend about 3 cm below the radial tuberosities, and are well developed. The *M. supinator* insertion areas are smooth.

The proximal end of the left radius is generally larger and more robust than the right (in the head, neck and radial tuberosity dimensions: Table 12), but the right clearly has a greater development of the interosseous crest and shaft.

The shafts are relatively straight (in both anterior and lateral views) and are of moderate robusticity (Table 13). The *M. pronator teres* insertions are clearly defined and of moderate rugosity. The attachment sites for *M. pronator quadratus* and *M. brachioradialis* are too damaged on the left-side (and absent on the right) to say anything about. On the dorsal aspect of the distal left shaft, the dorsal ('Lister's') tubercle is very well developed.

Table 13 Comparative radial osteometrics (mean, SD, n).

	Gough's Cave 1	LUP/Meso ♂	LUP/Meso ♀
Right radii			
Midshaft AP diam	12.0	12.3, 0.4, 4	10.1, 0.9, 3
Midshaft ML diam	16.9	16.0, 1.4, 4	13.3, 1.8, 3
Head-neck length	33.0	31.8, 2.6, 12	31.9, 1.7, 5
Neck-shaft angle	6°	8.8°, 3.4,12	11.1°, 5.1, 6
Head AP diam	21.1	22.7, 1.4, 8	20.8, 1.7, 3
Head ML diam	21.2	21.8, 1.4, 10	20.6, 1.8, 3
Neck AP diam	14.7	23.2, 1.2, 10	11.9, 1.4, 6
Neck ML diam	12.4	13.3, 1.3, 9	11.3, 1.0, 6
Bicip. Tuberosity length	22.4	21.8, 2.6, 12	22.0, 2.6, 7
Bicip. Tuberosity breadth	14.1	14.5, 1.2, 12	12.4, 1.3, 7
Left radii		UP/Meso ♂	UP/Meso ♀
Maximum length[a]	248	243.9, 7.4, 10	226.8, 8.8, 4
Articular length[a]	235	228.5, 9.3, 13	215.2, 7.9, 5
Midshaft AP diam	11.9	11.9, 0.7, 4	10.0, 0.7, 3
Midshaft ML diam	15.1	14.9, 1.5, 4	12.5, 1.0, 3
Head-neck length	31.3	31.8, 1.7, 11	31.0, 3.3, 4
Neck-shaft angle	6°	9.0°, 4.1, 10	12.8°, 7.0, 5
Head AP diam	22.4	22.9, 1.0, 12	17.7, 4.0, 3
Head ML diam	21.3	21.7, 0.6, 8	18.9, 2.3, 4
Neck AP diam	15.1	14.0, 1.0, 12	12.4, 0.9, 6
Neck ML diam	14.7	12.3, 3.9, 14	11.4, 1.0, 6
Bicip. tubersoity length	21.5	22.2, 2.5, 13	19.4, 1.8, 6
Bicip. tuberosity breadth	14.2	14.0, 1.7, 14	12.7, 1.0, 7

All measurements are in millimeters and are defined in Table 12.
[a] includes estimated lengths for some comparative specimens.

Figs 9, 10 Gough's Cave 1 radii, in ventral (a), medial (b), dorsal (c) and lateral (d) views; **9,** right-side radius (note that the distal end is reconstructed); **10,** left-side radius; × 0.5.

COMPARATIVE MORPHOLOGY OF THE UPPER LIMB REMAINS

In most measures, the Gough's Cave 1 upper limb skeleton is comparable to that of other European males alive during the final Pleistocene and early Holocene. In both gross external and cross-sectional dimensions of the humerus, radius and ulna, Gough's Cave 1 is unremarkable compared to his contemporaries. These bones tend to be slightly longer (on average) than those of his male contemporaries, yet to have epiphyseal dimensions and diaphyseal diameters roughly equivalent to the mean values observed in the comparative sample males (Tables 7, 10 and 13). Thus relative to length, the upper limb long bones of Gough's Cave 1 are somewhat gracile when seen in the context of other similarly aged fossils. This characterization holds for size-standardized measures of the mechanical strength of the humerus and ulna as well (Tables 8 and 11), suggesting that the habitual biomechanical loads incurred in the upper limbs of Gough's Cave 1 were somewhat meager relative to other Upper Paleolithic and Mesolithic foragers.

Perhaps the most remarkable feature in the upper limbs (used here in the broad sense to include the pectoral girdles) is the robusticity of Gough's Cave 1's right clavicle. In terms of length, the right clavicle falls between the mean values for males and females in the comparative sample (Table 2). However, in external dimensions (Table 2) and unstandardized cross-sectional properties (Table 3), Gough's Cave 1's right clavicle tends to fall on or above the male sample means. The superoinferior, dorsoventral and maximum 2nd moments of area, as well as the polar moment of area, are two or more standard deviations above the (admittedly small) male sample means (Table 3). Given that Gough's Cave 1's claviculae were relatively short, the clavicular strength values are all the more striking. Consideration of the cross-sectional geometric properties presented in Table 3 shows that the large values for bending rigidity (2nd and polar moments of area) in Gough's Cave 1's right clavicle are due in part to the overall size of the cross-sections (TA). The right clavicle has a midshaft cortical area (CA) close to the comparative male mean, but this cortical bone is distributed further from the geometric centre of the section. This results in a relatively large medullary cavity, a relatively low percent cortical area, and relatively high 2nd moments of area.

A similar consideration of Gough's Cave 1's left clavicle shows it to be relatively gracile, at least in cross-sectional measures of strength (Table 3) if not in external dimensions (Table 2). Bilateral asymmetry in upper limb strength measures is certainly to be expected (see Churchill, 1994), and the degree of asymmetry seen here is not likely to be outside the range observed in fossil and recent, moderately to highly active foragers. What is curious about Gough's Cave 1 is the robusticity of the right clavicle in the context of an otherwise relatively gracile upper limb skeleton.

Gough's Cave 1's right clavicle has an I_x/I_y ratio that is above but within one standard deviation of the male comparative sample mean (yet below the mean of females: Table 3), yet has an I_{max}/I_{min} ratio considerably higher than the mean of the comparative samples. The angle formed between the plane of greatest bending rigidity and the dorsoventral plane passing through the centre of the section is 130° in the Gough's Cave 1 right clavicle, indicating an adaptation to bending in the superodorsal to inferoventral direction (*i.e.*, about an inferodorsal to superoventral axis). This might suggest an habitual generation of dorsoventrally oriented forces operating on the clavicle during full abduction of the humerus (in which scapular rotation on the thorax necessitates conjunct posterior axial rotation of the clavicle, bringing the superodorsal-inferoventral axis of the bone into the transverse plane of the body). While it is the case that the muscle scars for *M. deltoideus*, the major abductor of the humerus, are rugose on the clavicle (at least on the left side, this region is damaged in the right), scapulae and humeri, it is also the case that the humeral deltoid tuberosities are weakly developed. This, combined with the overall gracility of the other upper limb bones, makes it difficult to imagine a behavior pattern that could differentially load the clavicle more than the other bones of the limb. The asymmetry evident in the claviculae is also not apparent in the other upper limb remains (and in fact the reverse pattern is seen in the radii, with the left being slightly more robust than the right).

Actions involving forceful right-side scapular abduction (as in pushing on a heavy object with the arms abducted and flexed, that is, out in front of the body) or adduction (as in forcefully pulling something using motion at the shoulder) would be expected to generate bending moments in the transverse plane of the clavicle. However, such movements would also be expected to create bending stresses in the arm and forearm. Thus if Gough's Cave 1 were routinely engaged in an activity requiring forceful pulling or pushing with one limb (perhaps involving woodworking in the manufacture of tools, or perhaps trap setting), we would expect a marked degree of right-left asymmetry in bone strength and muscle scarring in the upper limbs overall. Occupationally induced habitual heavy loading of the bones and joints of the upper limb is known to promote clavicular robusticity. For example, Lane (1887) reported marked robusticity in the *lateral half* of the clavicle in milkmen that routinely carried heavy milk pails with their arms by their sides. While observations like this support the possibility that the robusticity of the Gouch's Cave 1 right clavicle reflects habitual labor induced ('occupational') loads, the nature of the robusticty (both in terms of bone shape and the observed asymmetry) and the lack of associated degenerative changes to the clavicular joints does not fit with known patterns of occupational changes to upper limb morphology (reviewed in Kennedy, 1989). Thus the behavior patterns that produced this morphology in Cheddar Man remain, for the time being, unknown.

REFERENCES

Billy, G. 1969. Le squelette post-cranien de l'Homme de Chancelade. *L'Anthropologie*, **73:** 207–246.

Bonin, G. von 1935. The Magdalenian Skeleton from Cap-Blanc in the Field Museum of Natural History. *University of Illinois Bulletin*, **34:** 1-76.

Boule, M. & Vallois, H. 1937. Anthropologie. *In*: M. Péquart, S.-J. Péquart, M. Boule and H. Vallois (editors), *Téviec: Station-nécropole Mésolithique du Morbihan. Archives de l'Institute de Paléontologie Humaine*, Mémoire **18:** 111–227.

—— & —— 1946. *Les Hommes Fossiles*. Paris.

Churchill, S. E. 1994. *Human Upper Body Evolution in the Eurasian Later Pleistocene*. Ph.D. thesis, University of New Mexico.

—— 1996. Neanderthal scapular axillary border morphology revisited. *American Journal of Physical Anthropology* **Supplement 22:** 85 (abstract).

Dutour, O. 1986. Enthesopathies (lesions of muscular insertions) as indicators of the activities of Neolithic Saharan populations. *American Journal of Physical Anthropology* **71:** 221–224.

Endo, B. 1971. Some characteristics of the deltoid tuberosity of the humerus in the West Asian and European 'classic' Neanderthals. *Journal of the Anthropological Society of Nippon* **79:** 249–258.

Eschman, P. N. 1990. *SLCOMM*. Albuquerque.

Frayer, D. W. 1992. *The persistence of Neanderthal features in post-Neanderthal Europeans. In*: Bräuer, G. & Smith, F. H. (editors), *Continuity or Replacement: Controversies in Homo sapiens Evolution*: 171–180. Rotterdam.

Genet-Varcin, E. & Miquel, M. 1967. Contribution à l'étude du squelette magdalénien de l'abri Lafaye à Bruniquel (Tarn et Garonne). *Anthropologie, Paris*, **71:** 467-478.

Gieseler, W. von 1977. *Das jungpaläolithische Skelett von Neuessing. In*: Schröter, P. (editor), *75 Jahre Anthropologishe Staatssammlung München*: 39-51, München.

Graziosi, P. 1962. Découverte de gravures rupestres de type paléolithique dans l'Abri del Romito (Italie). *Anthropologie, Paris*, **66:** 262-268.

Grazzini, E. 1921. Ossa umane del Paleolitico Superiore di Grotta Romanelli (Lecce). *Archo Antropolgia e Etnologia* **51:** 185-188.

Hawkey, D. E. & Merbs, C. F. 1995. Activity-induced musculoskeletal stress markers (MSM) and subsistence strategy changes among ancient Hudson Bay Eskimos. *International Journal of Osteoarchaeology*, **5:** 324–338.

Kennedy, K. A. R. 1989. Skeletal markers of occupational stress. *In*, M. Y. Iscan and K. A. R. Kennedy (editors), *Reconstruction of Life from the Skeleton*: 129–160. New York.

Lacam, R., Niederlender, A. & Vallois, H. V. 1944. Le gisement mésolithique du Cruzoul de Gramat. *Archives de l'Institute de Paléontologie Humaine*, Mémoire **21:** 1–92.

Lane, W. A. 1887. The causation of several variations and congenital abnormalities in the human skeleton. *Journal of Anatomy and Physiology*, **21:** 586–610.

Martin, R. 1928. *Lehrbuch der Anthropologie, 2nd Edition*. Jena.

McCown, T. D. & Keith, A. 1939. *The Stone Age of Mount Carmel II: The Fossil Human Remains from the Levalloiso-Mousterian*. Oxford.

McHenry, H. M., Corruccini, R. S. & Howell, F. C. 1976. Analysis of an Early Hominid Ulna from the Omo Basin. *American Journal of Physical Anthropology*, **44:** 295-304.

Nagurka, M. L. & Hayes, W. C. 1980. An interactive graphics package for calculating cross-sectional properties of complex shapes. *Journal of Biomechanics*, **13:** 59-64.

Paoli, G., Parenti, R. & Sergi, S. 1980. *Gli Scheletri Mesolitici della Caverna delle Arene Candide (Liguria)*. Memorie dell'Istituto Italiano di Paleontologia Umana, **3**. Rome.

Péquart, M. & Péquart, St. J. 1934. La nécropole mésolithique de L'ile d'Hoëdic, Morbihan. *Anthropologie, Paris*, **44:** 1–20.

Pittard, E. & Sauter, M. R. 1945. Un squelette magdalénien provenant de la station des Grenouilles (Veyrier, Haute-Savoie). *Archives suisses d'Anthropologie générale*, **11:** 149-200.

Sauter, M. R. 1957. Étude des vestiges osseux humains des grottes préhistoriques de Farincourt (Hte Marne, France). *Archives suisses d'Anthropologie générale*, **22:** 6.

Stasi, P. E. & Regalia, E. 1904. Grotta Romanelli (Castro, Terra d'Otranto). Stazione con faune interglaciali calda e di steppa. *Archivio per l'Antropologia e la Etnologia*, **34:** 29-30, 39.

Trinkaus, E. 1977. A functional interpretation of the axillary border of the Neandertal scapula. *Journal of Human Evolution*, **6:** 231-234.

Vallois, H. V. 1941-1946. Nouvelles recherches sur le squelette de Chancelade. *Anthropologie, Paris*, **50:** 65-202.

—— 1972. Le gisement et le squelette de Saint-Germain-la-Rivière – Troisième Partie – Anthropologie. *Archives de l'Institute de Paléontologie Humaine*, Mémoire **34**.

Verworn, M., Bonnet, R. & Steinmann, G. 1919. *Der diluviale Menschenfund von Oberkassel bei Bonn*: 6-10, Wiesbaden.